Characterization of single-file flow through human retinal parafoveal capillaries using an adaptive optics scanning laser ophthalmoscope

Johnny Tam,[1,*] Pavan Tiruveedhula,[2] and Austin Roorda[1,2]

[1]*Joint Graduate Group in Bioengineering, University of California, Berkeley and University of California, San Francisco, rm 485 Minor Hall; Berkeley, CA 94720-2020, USA*
[2]*School of Optometry, University of California, Berkeley, rm 485 Minor Hall; Berkeley, CA 94720-2020, USA*
*johnny@berkeley.edu

Abstract: Adaptive Optics Scanning Laser Ophthalmoscopy was used to noninvasively acquire videos of single-file flow through live human retinal parafoveal capillaries. Videos were analyzed offline to investigate capillary flow dynamics. Certain capillaries accounted for a clear majority of leukocyte traffic (Leukocyte-Preferred-Paths, LPPs), while other capillaries primarily featured plasma gap flow (Plasma-Gap-Capillaries, PGCs). LPPs may serve as a protective mechanism to prevent inactivated leukocytes from entering exchange capillaries, and PGCs may serve as relief valves to minimize flow disruption due to the presence of a leukocyte in a neighboring LPP.

OCIS codes: (110.1080) Active or adaptive optics; (170.4460) Ophthalmic optics and devices; (170.1470) Blood or tissue constituent monitoring; (110.2960) Image analysis.

References and links

1. B. W. Zweifach, *Functional Behavior of the Microcirculation* (Charles C Thomas, Springfield, Illinois, 1961).
2. J. C. Hogg, and C. M. Doerschuk, "Leukocyte traffic in the lung," Annu. Rev. Physiol. **57**(1), 97–114 (1995).
3. G. W. Schmid-Schönbein, R. Skalak, S. Usami, and S. Chien, "Cell distribution in capillary networks," Microvasc. Res. **19**(1), 18–44 (1980).
4. B. W. Zweifach, "Quantitative studies of microcirculatory structure and function. I. Analysis of pressure distribution in the terminal vascular bed in cat mesentery," Circ. Res. **34**(6), 843–857 (1974).
5. J. A. Martin, and A. Roorda, "Pulsatility of parafoveal capillary leukocytes," Exp. Eye Res. **88**(3), 356–360 (2009).
6. B. W. Zweifach, "Quantitative studies of microcirculatory structure and function. II. Direct measurement of capillary pressure in splanchnic mesenteric vessels," Circ. Res. **34**(6), 858–866 (1974).
7. A. S. Popel, and P. C. Johnson, "Microcirculation and Hemorheology," Annu. Rev. Fluid Mech. **37**(1), 43–69 (2005).
8. H. H. Lipowsky, "Microvascular rheology and hemodynamics," Microcirculation **12**(1), 5–15 (2005).
9. G. W. Schmid-Schönbein, Y. Y. Shih, and S. Chien, "Morphometry of human leukocytes," Blood **56**(5), 866–875 (1980).
10. J. Ben-nun, "Comparative flow velocity of erythrocytes and leukocytes in feline retinal capillaries," Invest. Ophthalmol. Vis. Sci. **37**(9), 1854–1859 (1996).
11. W. M. Kuebler, G. E. H. Kuhnle, J. Groh, and A. E. Goetz, "Leukocyte kinetics in pulmonary microcirculation: intravital fluorescence microscopic study," J. Appl. Physiol. **76**(1), 65–71 (1994).
12. E. R. Damiano, and T. M. Stace, "Flow and deformation of the capillary glycocalyx in the wake of a leukocyte," Phys. Fluids **17**(3), 031509 (2005).
13. J. M. Fitz-Gerald, "Plasma motions in narrow capillary flow," J. Fluid Mech. **51**(03), 463–476 (1972).
14. A. R. Pries, T. W. Secomb, P. Gaehtgens, and J. F. Gross, "Blood flow in microvascular networks. Experiments and simulation," Circ. Res. **67**(4), 826–834 (1990).
15. G. W. Schmid-Schönbein, S. Usami, R. Skalak, and S. Chien, "The interaction of leukocytes and erythrocytes in capillary and postcapillary vessels," Microvasc. Res. **19**(1), 45–70 (1980).
16. D. W. Sutton, and G. W. Schmid-Schönbein, "Elevation of organ resistance due to leukocyte perfusion," Am. J. Physiol. **262**(6 Pt 2), H1646–H1650 (1992).
17. J. A. Martin, and A. Roorda, "Direct and non-invasive assessment of parafoveal capillary leukocyte velocity," Ophthalmology **112**(12), 2219–2224 (2005).
18. Y. Zhang, S. Poonja, and A. Roorda, "MEMS-based adaptive optics scanning laser ophthalmoscopy," Opt. Lett. **31**(9), 1268–1270 (2006).

19. A. Roorda, F. Romero-Borja, W. Donnelly III, H. Queener, T. J. Hebert, and M. C. W. Campbell, "Adaptive optics scanning laser ophthalmoscopy," Opt. Express **10**(9), 405–412 (2002).
20. J. Tam, J. A. Martin, and A. Roorda, "Noninvasive visualization and analysis of parafoveal capillaries in humans," Invest. Ophthalmol. Vis. Sci. **51**(3), 1691–1698 (2010).
21. L. Laatikainen, and J. Larinkari, "Capillary-free area of the fovea with advancing age," Invest. Ophthalmol. Vis. Sci. **16**(12), 1154–1157 (1977).
22. D. M. Snodderly, R. S. Weinhaus, and J. C. Choi, "Neural-vascular relationships in central retina of macaque monkeys (*Macaca fascicularis*)," J. Neurosci. **12**(4), 1169–1193 (1992).
23. E. Evans, and Y. C. Fung, "Improved measurements of the erythrocyte geometry," Microvasc. Res. **4**(4), 335–347 (1972).
24. G. A. Lutty, J. Cao, and D. S. McLeod, "Relationship of polymorphonuclear leukocytes to capillary dropout in the human diabetic choroid," Am. J. Pathol. **151**(3), 707–714 (1997).
25. P. K. Yu, C. Balaratnasingam, S. J. Cringle, I. L. McAllister, J. Provis, and D. Y. Yu, "Microstructure and network organisation of the microvasculature in the human macula," Invest. Ophthalmol. Vis. Sci. **51**(12) 6735–6743 (2010).
26. I. C. Michaelson, *Retinal Circulation in Man and Animals* (Charles C Thomas, Springfield, Illinois, USA, 1954).
27. D. Kleinfeld, P. P. Mitra, F. Helmchen, and W. Denk, "Fluctuations and stimulus-induced changes in blood flow observed in individual capillaries in layers 2 through 4 of rat neocortex," Proc. Natl. Acad. Sci. U.S.A. **95**(26), 15741–15746 (1998).
28. B. W. Zweifach, D. B. Metz, and E. R. Clark, "Selective distribution of blood through the terminal vascular bed of mesenteric structures and skeletal muscle," Angiology **6**(4), 282–290 (1955).
29. A. G. Hudetz, "Blood flow in the cerebral capillary network: a review emphasizing observations with intravital microscopy," Microcirculation **4**(2), 233–252 (1997).
30. E. Friedman, T. R. Smith, and T. Kuwabara, "Retinal Microcirculation in vivo," Invest. Ophthalmol. **3**, 217–226 (1964).
31. R. Flower, E. Peiretti, M. Magnani, L. Rossi, S. Serafini, Z. Gryczynski, and I. Gryczynski, "Observation of erythrocyte dynamics in the retinal capillaries and choriocapillaris using ICG-loaded erythrocyte ghost cells," Invest. Ophthalmol. Vis. Sci. **49**(12), 5510–5516 (2008).
32. P. S. Jensen, and M. R. Glucksberg, "Regional variation in capillary hemodynamics in the cat retina," Invest. Ophthalmol. Vis. Sci. **39**(2), 407–415 (1998).
33. H. Nishiwaki, Y. Ogura, H. Kimura, J. Kiryu, K. Miyamoto, and N. Matsuda, "Visualization and quantitative analysis of leukocyte dynamics in retinal microcirculation of rats," Invest. Ophthalmol. Vis. Sci. **37**(7), 1341–1347 (1996).
34. D. A. Nelson, S. Krupsky, A. Pollack, E. Aloni, M. Belkin, I. Vanzetta, M. Rosner, and A. Grinvald, "Special report: Noninvasive multi-parameter functional optical imaging of the eye," Ophthalmic Surg. Lasers Imaging **36**(1), 57–66 (2005).
35. M. Paques, B. Boval, S. Richard, R. Tadayoni, P. Massin, O. Mundler, A. Gaudric, and E. Vicaut, "Evaluation of fluorescein-labeled autologous leukocytes for examination of retinal circulation in humans," Curr. Eye Res. **21**(1), 560–565 (2000).
36. H. M. Becker, M. Chen, J. B. Hay, and M. I. Cybulsky, "Tracking of leukocyte recruitment into tissues of mice by in situ labeling of blood cells with the fluorescent dye CFDA SE," J. Immunol. Methods **286**(1-2), 69–78 (2004).
37. G. W. Schmid-Schönbein, K. L. Sung, H. Tözeren, R. Skalak, and S. Chien, "Passive mechanical properties of human leukocytes," Biophys. J. **36**(1), 243–256 (1981).
38. American National Standard for the Safe Use of Lasers, ANSI Z136.1–2007 (American National Standard Institute, New York, 2007).
39. K. Y. Li, P. Tiruveedhula, and A. Roorda, "Intersubject variability of foveal cone photoreceptor density in relation to eye length," Invest. Ophthalmol. Vis. Sci. **51**(12), 6858–6867 (2010).
40. D. W. Arathorn, Q. Yang, C. R. Vogel, Y. Zhang, P. Tiruveedhula, and A. Roorda, "Retinally stabilized cone-targeted stimulus delivery," Opt. Express **15**(21), 13731–13744 (2007).
41. C. R. Vogel, D. W. Arathorn, A. Roorda, and A. Parker, "Retinal motion estimation in adaptive optics scanning laser ophthalmoscopy," Opt. Express **14**(2), 487–497 (2006).
42. J. Tam, and A. Roorda, "Enhanced detection of cell paths in spatiotemporal plots for noninvasive microscopy of the human retina," in *2010 IEEE International Symposium on Biomedical Imaging: From Nano to Macro* (IEEE, 2010) , pp. 584–587.
43. J. Tam, and A. Roorda, "Speed quantification and tracking of moving objects in adaptive optics scanning laser ophthalmoscopy," J. Biomed. Opt. (to be published).
44. C. E. Riva, and B. Petrig, "Blue field entoptic phenomenon and blood velocity in the retinal capillaries," J. Opt. Soc. Am. **70**(10), 1234–1238 (1980).
45. M. Meinke, G. Müller, J. Helfmann, and M. Friebel, "Optical properties of platelets and blood plasma and their influence on the optical behavior of whole blood in the visible to near infrared wavelength range," J. Biomed. Opt. **12**(1), 014024 (2007).
46. T. Nagaoka, and A. Yoshida, "Noninvasive evaluation of wall shear stress on retinal microcirculation in humans," Invest. Ophthalmol. Vis. Sci. **47**(3), 1113–1119 (2006).

1. Introduction

The flow of individual cells through capillary networks is dependent on a number of interacting factors, including metabolic demand and organ-specific factors [1,2], network topology [3], heart rate [4–6], and the presence and distribution of erythrocytes and leukocytes [7,8]. Although erythrocytes outnumber leukocytes by a ratio of about 1000:1, the role of leukocytes in the microcirculation is particularly important, because leukocytes are larger and less deformable than erythrocytes [9], and thus travel significantly slower through the microcirculation [10,11]. The transit of leukocytes through narrow capillaries compresses the glycocalyx [12] and upsets the normally faster-moving erythrocytes [10], creating a plasma zone immediately upstream of the leukocyte [13] with a corresponding erythrocyte train immediately downstream [14,15]. Further upstream, at the prior branch point, the channel of higher flow [3] may shift from one branch to the other as the flow resistance is temporarily increased in the branch containing the leukocyte [16]. Thus, there is a dynamic interaction between leukocytes and erythrocytes in capillary networks, particularly at the level of single-file flow. It is important to characterize the nature of single-file flow to better understand diseases that affect the microcirculation, such as diabetic retinopathy.

The human parafoveal capillary network, a highly organized system residing in the inner layers of the retina, can be observed noninvasively and in situ using an Adaptive Optics Scanning Laser Ophthalmoscope (AOSLO) [17–20]. Of particular interest is the terminal capillary network near the fovea, marked by the foveal avascular zone (FAZ), a zone approximately 500-600 microns in diameter that is free of vascularization in the inner retina [21]. Immediately outside the FAZ, the parafoveal capillaries are single-layered and planar [22]. Flow is necessarily single-file. Erythrocytes, which have a mean major diameter of 7.82 μm [23], lymphocytes, with diameters of 5.75 μm, and neutrophils, monocytes, and eosinophils, with diameters of 7.25 μm [9], must squeeze through narrow parafoveal capillaries with lumen diameters of 3.5-6 μm [24]. This network is fed by interdigitating arterioles and venules oriented in directions normal to the FAZ contour; in contrast, the capillaries are preferentially oriented in directions tangential to the FAZ contour [22,25]. Immediately exterior to each arteriole, there is a zone of reduced capillary density; farther from the arteriole, the capillary density gradually increases, reaching a maximum at the location of each venule [26]. These observations show that at the cellular level, the parafoveal capillary network is locally heterogeneous.

The distribution of individual blood cells in capillary networks is also heterogeneous, both spatially across different capillaries [3], and temporally within the same capillary [27]. At a bifurcation spawning two daughter vessels of unequal flow, the distribution function of erythrocytes is highly nonlinear [3]. Thoroughfare channels, which connect terminal arterioles to collecting venules, contain high volumes of blood flow relative to neighboring capillaries [28,29]. The remaining capillaries have been termed exchange, or true capillaries, through which a normal ebb and flow of cells can sometimes be observed [29]. In many capillary networks, flow is regulated by precapillary sphincters; however, this does not appear to be the case in the cat retina [30]. Erythrocytes have been observed to fluctuate in both concentration and flow direction in the cat retina [30], and spontaneously pause during flow through monkey retinal capillaries [31]; however, a separate study using invasive endoscopy found variations in erythrocyte speed in cat retinal capillaries, but no evidence of plasma skimming, stasis, or intermittent flow [32]. Leukocytes have also been observed to preferentially flow through specific channels in the retina [33]. These peculiarities can be lost with ex-vivo approaches. To our knowledge, the distribution of blood constituents in thoroughfare and exchange capillaries in humans has not yet been characterized in vitro.

It is important to utilize a noninvasive, in situ method to investigate the behavior of single cells in parafoveal capillaries, since any invasive method can potentially change the nature of flow, particularly at the level of single-file flow. Currently, most imaging methods for investigating the microcirculation are (i) invasive, (ii) require administration of a contrast agent, or (iii) cannot be performed in humans. A notable exception is the Retinal Function

Imager [34], which can investigate blood flow noninvasively in humans using intrinsic motion signals; however, there are two considerations. First, this method is limited to an imaging sequence consisting of 6 snapshots spaced 17 msec apart, for a total observation time of about 100 msec; and second, it is uncertain whether there is sufficient detail to examine the dynamic activity in the smallest capillaries. Another example, which is minimally invasive, uses fluorescein labeled autologous leukocytes to study flow dynamics in humans; however, the authors find evidence of leukocyte activation [35]. The process of removing, labeling, and reinserting leukocytes increases the spontaneous activation of leukocytes [36], which alters their mechanical properties [37], thereby changing the characteristics of the flow. We have recently described a method to noninvasively visualize human parafoveal capillaries using AOSLO videos acquired without administration of contrast agents [20].

In this paper, we illustrate a noninvasive method to characterize single-file flow through capillaries in a living human eye.

2. Materials and Methods

2.1 Human Subjects

The experiments described in this study were approved by the University of California, Berkeley Institutional Review Board. After detailed explanation of the procedures, written informed consent was obtained. We characterized the parafoveal capillary network from the right eye of a 24-year-old female subject with no history of ocular or systemic disease.

2.2 AOSLO Imaging
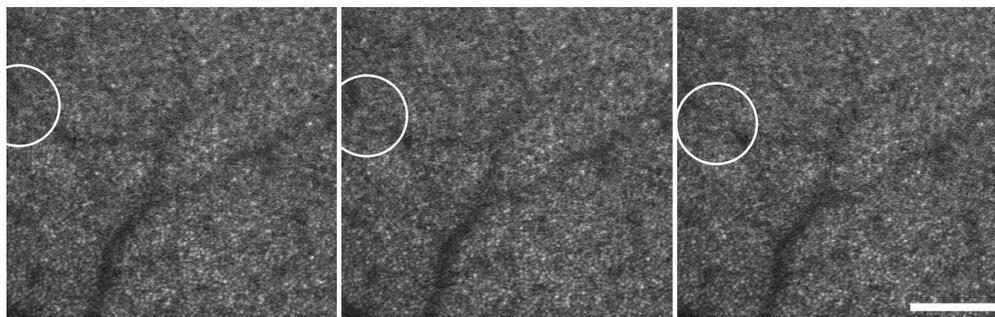
Fig. 1. Three consecutive frames showing a low contrast leukocyte (circled) moving through a human parafoveal capillary. The spatial contrast is very low, since no contrast agents are used; however, by examining consecutive frames, the motion of individual leukocytes can be detected. Small circular dots are photoreceptors. Frames have been corrected for scanning distortion and eye motion. Scale bar, 100 μm.

AOSLO videos were acquired as described previously using parameters that were optimized for blood flow imaging [20] (Fig. 1). One important parameter is the selection of an appropriate plane of focus. It is advantageous to acquire images near the photoreceptor layer, since this layer contains high contrast spatial features that are useful for stabilizing videos to correct for eye motion. However, since the inner capillary layers reside anterior to the photoreceptors, it is also advantageous to acquire images near the capillary layers, to maximize both the sharpness of the resulting vascular images and also the motion contrast of the individual cells. Thus, we selected a plane of focus that was slightly anterior to the photoreceptor layer. The right eye of the subject was dilated (2.5% phenylephrine hydrochloride, 1% Tropicamide). A total of 76 overlapping videos were acquired in one 2 hour session, with 9 videos acquired near the FAZ (40 second videos with 1.5° field sizes), and 68 videos farther from the FAZ (15 second videos with 1.8° field sizes), for a combined field of approximately 6.5° x 9.5° (height and width). Videos were acquired at 60 fps, using an 840 nm super luminescent diode. The AOSLO normally acquires images at 30 fps, using the forward sweep of a fast resonant scanner that operates at 16 kHz; to achieve 60 fps, we incorporated both the forward and return sweeps of the scanner. To insure safe light levels, we

maintained an exposure level that was more than 10x below the Maximum Permissible Exposure limit defined by the American National Standards Institute [38]. There was no injection of a contrast agent.

2.3 Pulse Measurements

A photoplethysmograph (MED Associates Inc., St. Albans, VT, USA) was attached to the subject's thumb, and the output was continuously recorded in a data file during video recordings. The output was simultaneously analyzed in real-time to detect the location of the largest peak of the pulse waveform, and then encoded onto the video by marking the frame at which the detection occurred with a small white square (referred to as a "pulse blip" in the remainder of the manuscript). After the imaging session, the encoded blips were checked against the recorded data files to verify proper encoding.

2.4 Fundus Photography

A digital fundus camera was used to acquire a red-free photograph of the posterior pole of the right eye at a 30° field size (Zeiss Visucam NM/FA, Carl Zeiss Meditec Inc., Dublin, CA, USA).

2.5 Biometry Measurements

Axial length, anterior chamber depth, and corneal curvature were directly measured, after maximal dilation was achieved (IOL Master, Carl Zeiss Meditec Inc., Dublin, CA, USA). These measurements were used to make accurate conversions from visual angle to retinal distance [20,39], which were the units used in the spatiotemporal plot analysis.

2.6 Motion Contrast Enhancement
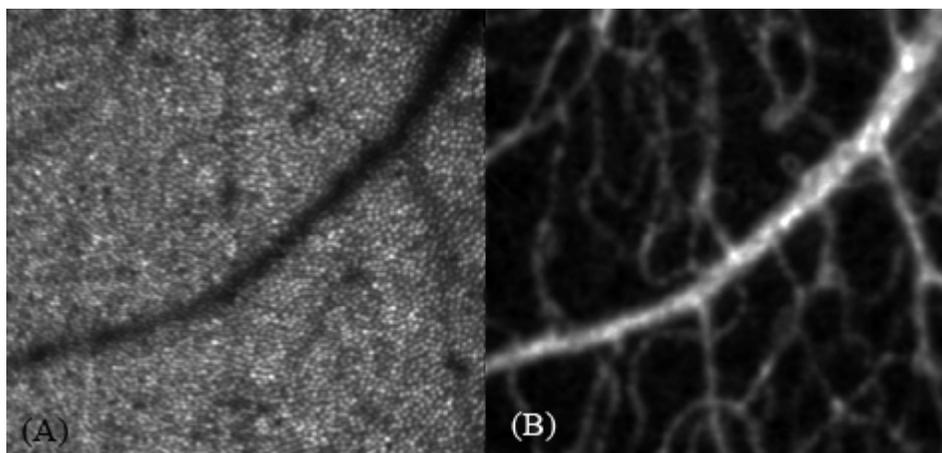
Fig. 2. Two different images generated from the same AOSLO video. (A) Photoreceptor image generated by calculating the average of all frames. (B) Capillary perfusion image generated by applying motion contrast enhancement.

AOSLO videos were processed to enhance the visualization of capillaries using motion contrast enhancement, as described previously [20]. We summarize the process briefly. Videos were preprocessed to correct for a scanning distortion due to the raster scanning, and then stabilized to correct for eye motions that cause inter- and intraframe distortions [40,41]. Next, motion contrast enhancement was applied, which involves calculation of a division video and a standard deviation image. The division video eliminates static portions of each frame (e.g. photoreceptors), while emphasizing regions of high relative motion (e.g. moving parcels of flow due to individual blood cells). Information across the entire division video is combined by calculating the pixel-by-pixel standard deviation image. The resulting image is a

map of perfused vessels; an image of photoreceptors can also be recovered from the AOSLO video by calculation of the average image (Fig. 2).

2.7 Spatiotemporal Plots and Pulsatility Measurements

Spatiotemporal plots are a method to visualize the hemodynamics of capillaries by converting data from a three-dimensional representation (2 spatial, 1 temporal) to a two-dimensional representation (1 spatial, 1 temporal), by assuming knowledge about vessel locations. These plots can be generated offline from AOSLO videos, as described previously, and in the case of single-file flow, there is no loss of information during the conversion [42]. Briefly, for each vessel of interest, the vessel centerline is extracted from an image of perfused vessels [20], and then intensities along the extracted centerline are read off from the division video. These intensities are plotted against frame number (Fig. 3). An object that moves through the vessel generates a sloped trace on the spatiotemporal plot, starting at one end of the plot/vessel, and finishing at the other end. Artifacts due to blinks or failures to properly correct for eye motion are easily distinguished from actual signal due to blood flow, since they give rise to purely vertical lines on the spatiotemporal plots.
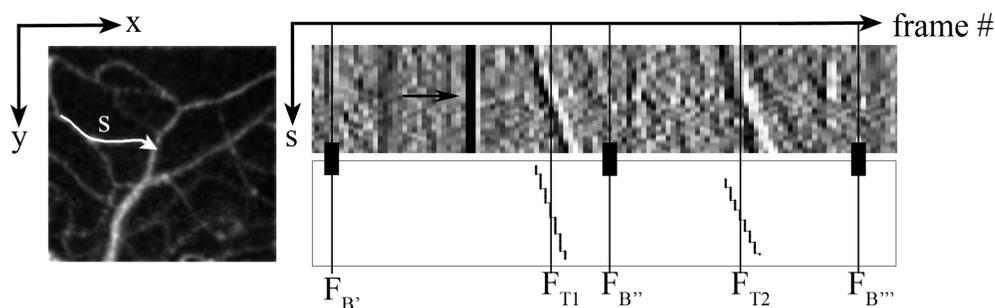
Fig. 3. Generation and analysis of a spatiotemporal plot from the AOSLO video shown in Fig. 1. A vessel centerline is identified on the image of perfused capillaries. Vessel coordinates are converted from *(x,y)* coordinates to *(s)* coordinates to reduce data by one spatial dimension. To generate the spatiotemporal plot, intensities along *s* are plotted for each frame of the division video. A 120-frame segment of the spatiotemporal plot for the selected vessel is shown. Sloped traces, which correspond to motion of fluid parcels, are manually extracted. Purely vertical traces are due to artifacts – one example, due to a blink, is shown (arrow). Two example traces that were extracted are shown. The extracted traces were analyzed to give information about flow direction, frequency, speed, and pulsatility as described in the text. F_{T1} and F_{T2} are the frames at which traces were extracted; $F_{B'}$, $F_{B''}$, and $F_{B'''}$ are the frames at which pulse blips occurred.

Sloped traces from the spatiotemporal plot were manually extracted to derive the following information about flow dynamics: frequency, flow direction, speed, and pulsatility. Frequency information could be computed by simply counting the number of extracted traces, and dividing by the length of the video. To compute flow direction of each trace, a linear regression was applied, and the sign (positive or negative) of the slope was used to determine the flow direction. The speed was quantified using a procedure described elsewhere that corrects for measurement errors due to raster scanning and eye motion [43]. Finally, to quantify pulsatility, a velocity waveform was generated using the encoded pulse blips. Since each pair of pulse blips corresponded to one pulse cycle, a velocity waveform could be generated by combining all pairs of pulse blips across a video. Speeds were plotted as a function of time relative to the pulse cycle, given by $(F_T - F_{B'}) / (F_{B''} - F_{B'})$, where F_T is the central frame of the extracted trace, and $F_{B'}$ and $F_{B''}$ are the frames of the pulse blips immediately preceding and following F_T. At the beginning of the video, when there is no preceding pulse blip, the timing is estimated by extrapolating from the next two pulse blips, given by $(F_T - F_{B''}) / (F_{B'''} - F_{B''})$, where $F_{B''}$ and $F_{B'''}$ are the frames of the next two pulse blips. A similar procedure is used at the end of the video, if there is no pulse blip after an extracted trace. This process normalizes measured speeds to the current heart rate, and is appropriate

when the heart rate stays reasonably constant for the duration of the recording session. To compute an averaged velocity waveform, the pulse cycle was divided into five equal segments, and data within each segment was averaged, as described previously [5]. These segments were used to compute the pulsatility index, given by $V_{max} - V_{min} / V_{mean}$, where V_{max} and V_{min} are the maximum and minimum calculated speeds across the entire video for a given vessel, and V_{mean} is the average [44].

3. Results

3.1 Vessel mapping
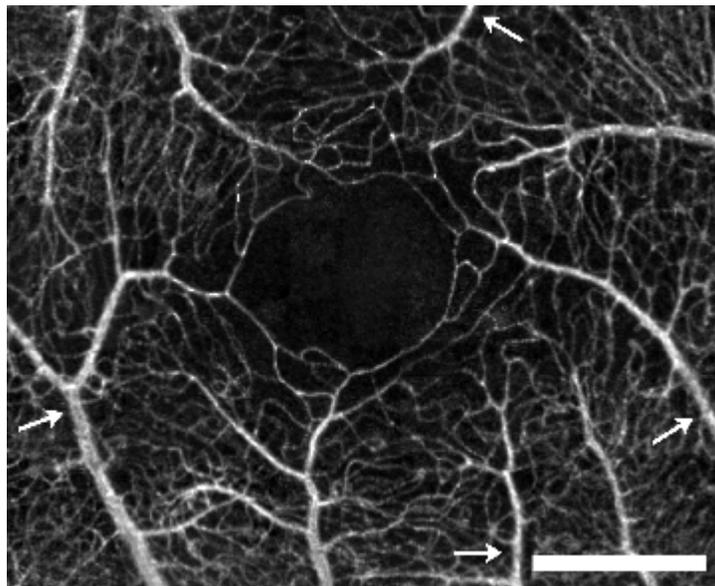
Fig. 4. Montage showing parafoveal capillaries generated by applying motion contrast enhancement to 76 overlapping AOSLO videos acquired noninvasively without contrast agent. Arrows denote arterioles. Scale bar, 500 μm.

A montage of parafoveal capillaries was generated by first applying motion contrast enhancement to each AOSLO video, and then combining overlapping images using image editing software (Adobe Photoshop; Adobe Systems, Inc., San Jose, CA, USA) (Fig. 4). For display purposes, image intensities were normalized and image borders were deleted. This had no effect on the spatiotemporal plot analysis, since we used non-edited images for the analysis of each video. Arterioles and venules were identified on a fundus photograph of the same eye by a retina specialist; identification of arterioles and venules on the AOSLO montage was then performed by overlaying the montage onto the fundus photograph (Fig. 5). We confirmed many features of the parafoveal capillary network that have been previously described: an FAZ, surrounded by a single layer of capillaries in the zone immediately outside the FAZ; interdigitation of arterioles and venules; arterioles and venules oriented in directions normal to the contour of the FAZ, and capillaries oriented tangentially. Although some arterioles exhibited reduced capillary density compared to venules, this effect was less apparent near the macular region, as previously reported [25].

3.2 Comparison to red-free fundus photography

Vessels were overlaid onto the red-free fundus photography for comparison (Fig. 5). Red-free fundus photography was the best option for visualization of vessels in the clinic for this subject, since fluorescein angiography, which involves injection of contrast agent, is not performed for subjects with no systemic or ocular disease. All vessels that could be identified

on the red-free were seen on the AOSLO image; the AOSLO image also showed additional capillaries that were not visible on the red-free fundus.
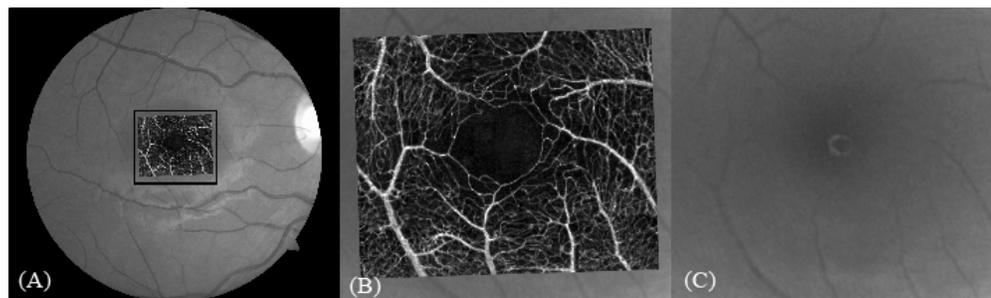
Fig. 5. Comparison of AOSLO with red free fundus photography. (A) AOSLO overlay on fundus photograph. The black box is magnified in panels (B) and (C).

3.3 Interpretation and analysis of spatiotemporal plots

There was considerable variation in the appearance of spatiotemporal plots (Fig. 6). In situations where contrast is generated invasively, interpretation of spatiotemporal plots is straightforward: traces on spatiotemporal plots correspond either to fluid gaps from injected dyes, or to individual cells from fluorescently-labeled cells. In the case of cell labeling, one can exactly verify the type of cell that is being analyzed. Since AOSLO images are acquired without contrast agents, direct verification is not possible. We present an interpretation of two unique patterns of the spatiotemporal plots, which we attribute to leukocytes and plasma gaps.

The first category of traces included those that were (i) thick, (ii) high contrast, (iii) sparse, and (iv) unidirectional. We classified these traces as leukocytes traces when all four criteria were met, for the following reasons. First, since leukocytes are larger than erythrocytes, they have a longer length in single-file flow; this corresponds to a thicker trace on the spatiotemporal plot. Second, as described earlier, the fluid mechanics model of single-file leukocyte flow features an erythrocyte-free plasma zone immediately upstream of the leukocyte, followed by an erythrocyte-packed zone immediately downstream. The size of the plasma and erythrocyte-packed zones are large compared to the size of normal red cell spacings in the absence of leukocytes [15]. At the imaging wavelength (840 nm), erythrocytes are strongly absorbing relative to plasma [45]. We suspect that leukocytes have low absorbance at near infrared. Taken together, these assumptions would lead to high contrast leukocyte traces on the spatiotemporal plots for single-file capillaries. Third, leukocytes were sparse, appearing only in a minority of frames, and absent in the majority of frames; this corresponds to sparse traces on the spatiotemporal plots. Finally, examining the videos directly, leukocytes were always observed to flow in a single direction, with no pausing or dwelling; this corresponds to unidirectional traces. By direct comparison of videos to spatiotemporal plots (i.e. by labeling videos with the coordinates of extracted traces), we verified that when these four conditions were met, extracted traces corresponded to leukocytes on AOSLO videos.

The second category of traces included those that were (i) thin and (ii) dense. We classified these traces as plasma gap traces. These traces tended to have lower contrast than leukocyte traces, which is consistent with direct observations of AOSLO videos, where leukocyte-type objects exhibit higher spatial contrast compared to higher frequency fluctuations that are due to other elements of blood flow. First, a thinner trace corresponds to an object that is shorter; thin traces are unlikely to correspond to leukocytes. This suggests that thin traces are due to either individual erythrocytes or to plasma gaps between erythrocytes. However, since the density of erythrocytes in capillary flow is high, we do not expect to have the spatial and temporal resolution to reliably visualize the motion of individual erythrocytes. Second, denser traces correspond to higher frequencies. Many of the

thin traces occurred at frequencies that were too high to be generated by leukocytes. Some of these traces also exhibited some evidence of bidirectionality (i.e. reversal of flow direction).
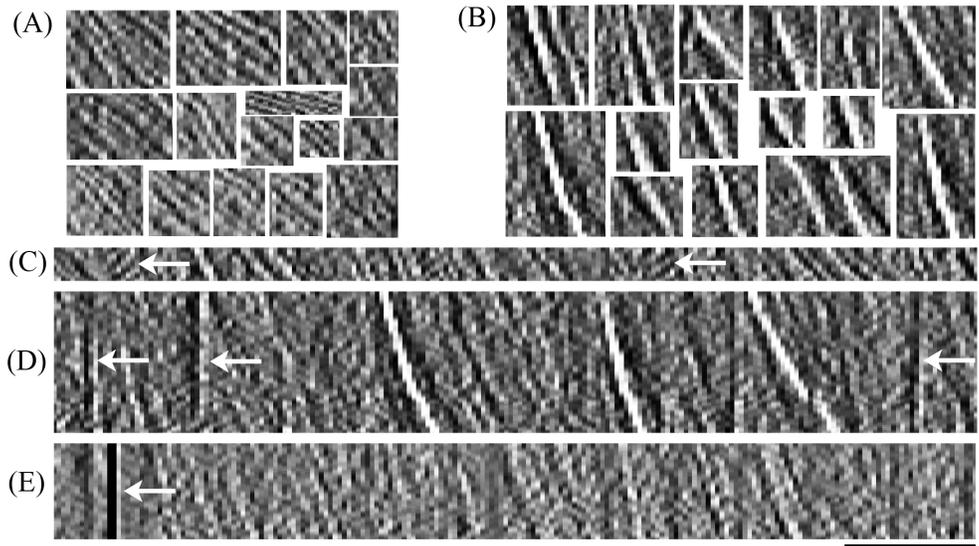
Fig. 6. Interpretation of spatiotemporal plots, showing representative traces due to (A) plasma gaps and (B) leukocytes. These traces were isolated from full spatiotemporal plots to illustrate the two categories of traces that were identified for analysis. Plasma gap traces are thin and dense, while leukocyte traces are thick, high contrast, sparse, and unidirectional. 200-frame segments of spatiotemporal plots are shown from capillary segments that were identified as a (C) PGC, (D) LPP, and (E) neither a PGC nor a LPP. Note the areas of apparent bidirectionality in the PGC (arrow in C), and artifacts due to poor stabilization when correcting for eye motion (arrows in D) and a blink (arrow in E). Vertical scale bar, 0.5 mm; Horizontal scale bar, 0.5 seconds.

3.4 Identification of Leukocyte-Preferred Paths and Plasma-Gap Capillaries

Spatiotemporal plots were generated for selected capillary segments near the FAZ, and analyzed for leukocytes and plasma gaps. A total of 114 traces due to leukocytes and 1711 traces due to plasma gaps were identified across 21 capillary segments. We confirmed that the distribution of leukocytes and plasma gaps across the parafoveal network was not uniform.

Leukocyte traffic was not observed through most capillaries. To investigate the distribution of leukocytes, we calculated the frequency of leukocyte flow for each capillary segment, and then generated a histogram showing the distribution of leukocyte frequencies across all capillary segments (Fig. 7). Capillaries tended to either have very few leukocytes (non leukocyte-preferred-paths, non-LPPs), or have many leukocytes (leukocyte-preferred-paths, LPPs); we arbitrarily drew a line in the histogram to separate non-LPPs and LPPs. Next, we labeled non-LPPs and LPPs on a larger montage to show the spatial distribution of leukocyte flow, and found that LPPs were connected capillary segments that corresponded to a subset of thoroughfare channels, which were the simplest and most direct paths connecting arterial to venous circulations (Fig. 8).

Plasma gaps were observed in all capillaries, but the distribution was also nonuniform. First, we generated a histogram showing the frequency of plasma gaps across all capillary segments (Fig. 7). There was a clear separation in the histogram showing two capillary segments that exhibited steady plasma-gap patterns across the entire spatiotemporal plots (plasma gap capillaries, PGCs), shown to the right of the line in the histogram. Next, we labeled PGCs on a larger montage and found that PGCs were short capillary segments that served as anastomoses between more direct paths (Fig. 8).

To verify the computed flow directions, we also recorded the direction of flow for all the leukocytes, and found that they were in agreement with the direction of flow from arteries to veins as identified on the red-free fundus.
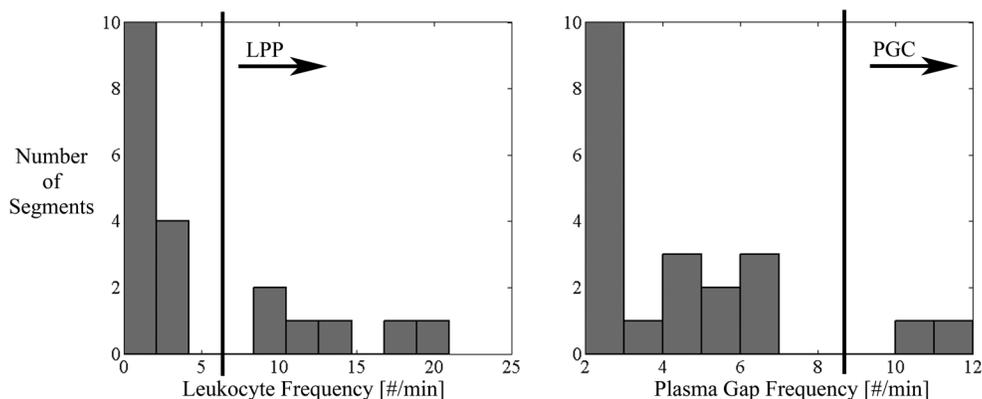
Fig. 7. Identification of leukocyte-preferred paths (LPPs) and plasma gap capillaries (PGCs). The distribution of leukocyte and plasma gap frequencies [#/min] are shown across all analyzed capillary segments. Vertical lines are inserted at breaks in the histograms to define LPPs and PGCs.
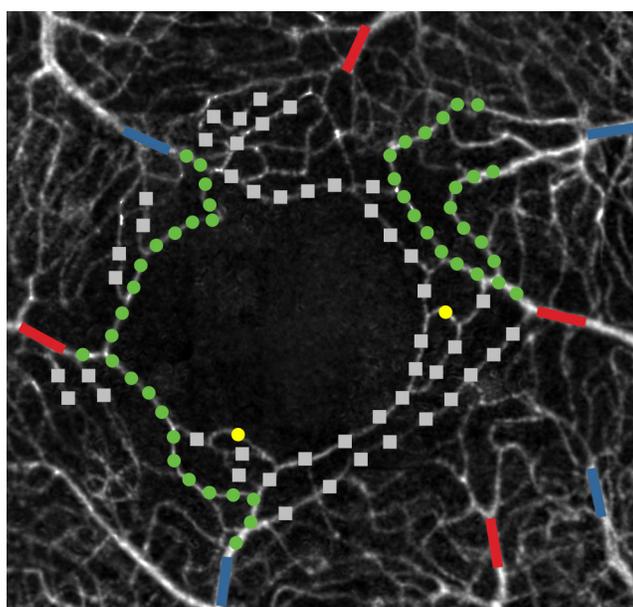
Fig. 8. Spatial distribution of LPPs (green), PGCs (yellow), and all others capillaries that were selected for analysis (gray). Terminal arterioles (red) and collecting venules (blue) are shown for reference.

3.5 Speed and pulsatility of leukocytes and plasma gaps

The speed of leukocytes and plasma gaps were similar in LPPs, and the pulsatility of leukocytes and plasma gaps were similar when considering all capillary segments.

To investigate speeds, we calculated the average speeds of leukocytes and plasma gaps. There was sufficient data to calculate plasma gap speeds across all vessels; however, for the leukocytes, only the six capillary segments corresponding to LPPs contained sufficient data for leukocyte speed quantification. All values are reported as mean +/− standard deviation.

Leukocytes had a speed of 1.80 +/− 0.22 mm/s (n = 114 leukocytes in 6 LPP segments), significantly higher than the speed of plasma gaps, which was 1.30 +/− 0.55 mm/s (n = 1711 plasma gaps in 21 capillary segments) (p<0.05). However, the speed of plasma gaps through the same 6 capillary segments selected for the leukocyte speed measurement was 1.73 +/− 0.28 mm/s (n = 311 plasma gaps in 6 LPP segments), which was not statistically different compared to the leukocyte speeds (p = 0.64).

To investigate pulsatility, we generated averaged velocity waveforms as a function of time relative to the pulse cycle. The pulse cycle was divided into five equal segments to generate an averaged waveform for the calculation of the pulsatility index (Fig. 9). We calculated pulsatility indices only when there was more than one speed measurement in each of the five segments. For the leukocytes, 2 out of 6 LPP segments satisfied these criteria; for the plasma gaps, there were 19 out of 21 capillary segments. There was no significant difference in the pulsatility indices for leukocytes, 0.54 +/− 0.05 (n = 45 leukocytes in 2 LPP segments), and plasma gaps, 0.61 +/− 0.14 (n = 1652 plasma gaps in 19 capillary segments) (p = 0.50). There was no apparent difference in pulsatility index across the capillary network.

The average heart rate across all videos was 55.9 +/− 4.3 bpm (n = 225 measurements).
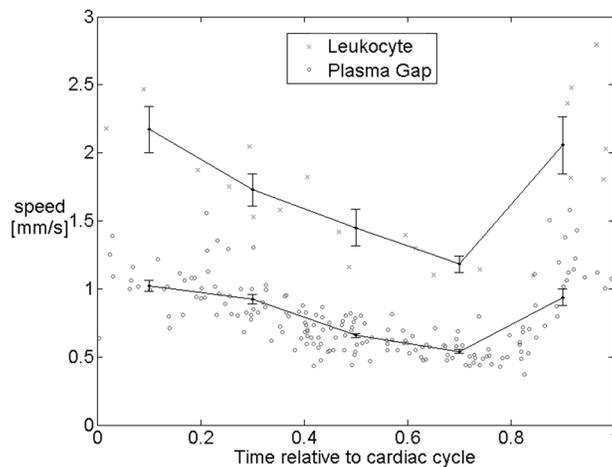
Fig. 9. Examples of averaged velocity waveforms for leukocytes in a single representative LPP segment (top) and plasma gaps in a single representative PGC (bottom), demonstrating the existence of pulsatility in capillaries with single-file flow. Data from extracted leukocytes and plasma gaps are averaged for five equal segments of the cardiac cycle to generate an averaged waveform.

4. Discussion

We demonstrate a noninvasive method to characterize single-file flow of leukocytes and plasma gaps through live retinal capillaries in the living human eye. Noninvasive methods are important to confirm previous reports of peculiarities in the microcirculation that have been observed using invasive methods. Motion contrast enhancement, combined with AOSLO, can be used to visualize and analyze the capillary network. We confirmed and quantified the distribution of leukocytes and plasma gaps across the network, and identified two specific types of capillaries. Leukocyte-preferred-paths (LPPs), a subset of thoroughfare channels, accounted for a clear majority of leukocyte traffic, and plasma-gap capillaries (PGCs), a subset of exchange capillaries, featured continuous flow of plasma gaps with occasional changes in flow direction. LPPs may be important as a protective mechanism to prevent leukocytes from entering non-LPP capillaries, where they can potentially become lodged, resulting in plugged capillaries. PGCs may be important for serving as relief valves for when a leukocyte enters a nearby LPP. Disruption of normal flow dynamics by neighboring leukocytes may be one of the factors that cause changes in the flow direction; spontaneous

changes in flow direction have been previously reported [27]. Thus, bidirectionality in PGCs may serve as an adaptive mechanism to minimize flow disruptions.

We also showed that both leukocytes and plasma gaps exhibit pulsatility. We report a pulsatility index of 0.54 and 0.61 for leukocytes and plasma gaps, which compares well to a previously published result using AOSLO data, which found a leukocyte pulsatility index of 0.45 +/− 0.09 [5]. A blue-field entoptic study reported a slightly higher pulsatility index of 0.98 in retinal capillaries, varying between 0.80 and 1.17 across 5 subjects [44]. These measurements may have been taken from larger capillaries, since the pulsatility index increases from small capillaries to large capillaries to small arterioles, and our measurements were taken at the level of the smallest capillaries. Noninvasive measurements of velocity waveforms in human retinal arterioles showed pulsatility indices of 1.13 for first order arterioles (those originating from the optic disc) and 0.93 for second order arterioles (those after the first branch point) [46].

Interestingly, leukocyte speeds appear to be significantly higher than plasma gap speeds when comparing the leukocytes found in LPPs to the plasma gaps found across all capillaries (p<0.05). However, since leukocytes could not be reliably identified in non-LPPs, this difference is likely skewed, since thoroughfare channels should have a higher flow speed than exchange capillaries. Indeed, there is no significant difference between leukocyte and plasma gap speeds when considering only the LPPs. Still, previous studies have reported that erythrocytes travel at a faster speed than leukocytes in the microcirculation. This suggests that either plasma gap speed is not a good proxy for erythrocyte speed, or leukocytes and erythrocytes do travel at similar speeds when restricted to only single-file capillaries. Inclusion of either pre-capillary arterioles or post-capillary venules would decrease measured leukocyte speeds, due to initial deformations needed to enter a narrow capillary, and leukocyte-vessel wall interactions, respectively. One study reported that the frequent attachments between leukocytes and the endothelium are disrupted by plasma fluid stresses upon entering single-file capillaries [15]. When examining the videos, no leukocytes were observed to pause at the level of single-file flow.

A clear limitation to using a noninvasive approach is that it is not possible to directly verify the types of cells that are being analyzed. This limitation is partly due to issues of low contrast. When imaging in humans, safety is a key consideration that limits the methods that can be applied. Thus, we needed to apply new methods to better visualize signals from plasma gaps and leukocytes. Due to noise and errors in frame-to-frame registration, the process of spatiotemporal analysis is subjective. We used a conservative approach by extracting only those elements that were clearly visible on the spatiotemporal plots. This results in under-extraction, but minimizes false extractions. Therefore, reported frequencies should not be interpreted as absolute measurements, but rather as relative measurements. Since the same criteria were applied across all spatiotemporal plots, comparisons can be made between vessels. To insure repeatability, we repeated the leukocyte extraction two times, and compared the percentages of leukocytes found in each vessel. Two months elapsed between analysis sessions to minimize memory effects for the analysis sessions, which require user interaction. The average absolute difference in leukocyte percentages was 1.2%, and the same LPPs were identified in both analysis sessions. Finally, to minimize bias, pulse blips were not displayed on spatiotemporal plots during extraction.

There are other important limitations. First, the imaging and data analysis procedures are time consuming, as they have not been fully optimized. Thus, the results presented in this work are for one healthy female subject. Future work will be performed to verify these results in additional eyes. Second, it is difficult to apply the methods to larger vessels, since larger vessels (i) tend to be out of the plane of focus, which decreases the visibility of flow through the vessel, and (ii) the spatial and temporal resolution requirements are higher for larger vessels compared to single-file flow in smaller capillaries. Third, the analysis method is difficult in regions of high capillary density, since it is difficult to identify sufficiently long capillary segments for generation of spatiotemporal plots. Fourth, it is possible that the analysis method detects aliased traces on the spatiotemporal plot, particularly when

interpreting regions where flow reverses direction. Finally, it is difficult to analyze motion due to individual erythrocytes, since the spatial density is high, which is disadvantageous for spatiotemporal plot analysis.

In this paper, we examined leukocytes and plasma gaps in single-file flow through retinal parafoveal capillaries, using a noninvasive approach. The major advantage of a noninvasive approach is that there is no potential disruption of the natural flow and cell distribution, which can be caused by spontaneous activation of normally inactivated leukocytes; the tradeoff is that direct verification of specific cell types is difficult. We identified two distinct categories of capillaries, one which accounted for the majority of leukocyte traffic (LPPs), and the other which primarily featured plasma gap flow (PGCs). LPPs may serve as a protective mechanism to prevent inactivated leukocytes from entering exchange capillaries, and PGCs may serve as relief valves to minimize flow disruption due to the presence of a leukocyte in a neighboring LPP. The noninvasive method presented in this paper may be useful for imaging fine vascular details such as microaneurysms and other capillary defects that manifest in retinal diseases, and for studying leukocytes in live human capillaries.

5. Acknowledgments